Opt Quant Electron (2015) 47:1311–1318
DOI 10.1007/s11082-014-0044-7

HOT mid-wave HgCdTe nBn and pBp infrared detectors

P. Martyniuk

Received: 25 September 2014 / Accepted: 7 October 2014 / Published online: 30 October 2014
© The Author(s) 2014. This article is published with open access at Springerlink.com

Abstract Narrow band gap photon infrared detectors require cryogenic cooling to suppress the noise deteriorating the performance. Among the competitive materials and theoretical predictions favouring type-II superlattices InAs/GaSb, HgCdTe has been still considered as the leader in terms of the fundamental physical parameters. The size, weight, power consumption and multispectral response of the infrared detection system play decisive role in fabrication of the higher operation temperature detectors. Several strategies have been implemented to improve the performance at elevated temperatures. The most efficient and used in HgCdTe technology are: non-equilibrium architectures and currently an idea of the barrier detectors. In this paper we present the comparison of the nB_nn and pB_pp (B_n and B_p stands for n/p-type doped barrier) HgCdTe photodetectors. pB_pp architecture allows to reach higher performance (detectivity $\sim 10^9$ cm Hz$^{1/2}$/W for $T = 200$ K) at mid-wave spectrum for wide range of absorber p-type doping $2 \times 10^{14} \rightarrow 10^{17}$ cm^{-3} and barrier Cd composition $0.37 \rightarrow 0.7$.

Keywords HOT · HgCdTe · BIRD · nB_nn · pB_pp

1 Introduction

Higher operation temperature (HOT) condition of the mid-wave (MWIR, 3–8 μm) infrared radiation (IR) photodetectors is one of the most important research area in infrared technology. The development of the new detector architectures have been driven by applications requiring multispectral detection, high frequency response, high detectivity, small size, low weight and power consumption (SWaP) and HOT conditions. The HgCdTe (mercury cadmium telluride-MCT) ternary alloy is a close to ideal infrared material system. Its position is conditioned by three key factors: Cd composition-dependent energy band gap, large optical coefficients that enable high quantum efficiency, favorable inherent recombination mecha-

P. Martyniuk (✉)
Institute of Applied Physics, Military University of Technology, 2 Kaliskiego Str., 00-908 Warsaw, Poland
e-mail: pmartyniuk@wat.edu.pl

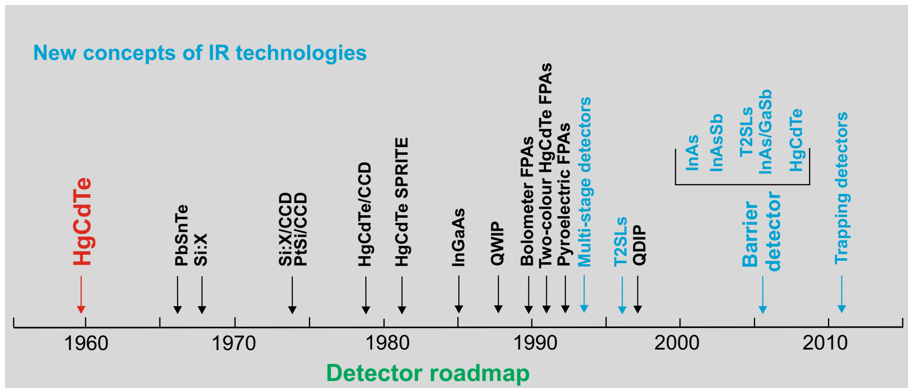

Fig. 1 Roadmap of IR detectors

nisms leading to long carrier lifetime and high operating temperature. In addition, extremely small change of lattice constant with composition makes it possible to grow high quality layered heterostructures (Norton 2002; Rogalski 2005). Because of its physical properties, HgCdTe has evolved to become the most important and versatile material and can be used for devices operating in various modes: photoconductors, photodiodes and metal-insulator-semiconductor (MIS) detectors (Piotrowski and Rogalski 2004, 2007). Additionally HgCdTe has inspired development of four generations of the IR detectors. The IR detector roadmap starting from 1959 when HgCdTe was used for the first time is shown in Fig. 1 (Rogalski 2011). The new concepts of IR technologies are marked in blue to include barrier detectors (barrier infrared detectors-BIRD), multi-stage, photon trapping detectors and type-II superlattices (T2SLs) with their potential to compete with HgCdTe.

Third generation HgCdTe systems are now implemented and concept of development of the fourth generation system is undertaken to include: multicolour capability, optical coupling (plasmonic), large number of pixels, high frame rates and high thermal resolution. A revolutionary emergence of focal plane arrays (FPAs) based on thermal detectors (bolometer, pyroelectric) has been observed but these devices are not expected to compete with the high-performance cryogenically cooled arrays or single photon detectors (see Fig. 1).

A number of concepts to improve HgCdTe IR detecors' performance have been proposed, but significant improvements in reduction of the dark current and increasing of the operating temperature has been reached by suppression of Auger thermal generation by implementing non-equilibrium conditions to the detectors structure (Ashley and Elliott 1985; Piotrowski et al. 2007). In practice, most of HgCdTe $N^+p(\pi)P^+$ Auger suppressed photodiodes are based on complex graded gap and doping multi-layer structures in which the transport of majority and minority carriers is determined by barriers. Additionally, p-type HgCdTe active regions are characterized by the best compromise between requirement of the high quantum efficiency and a low thermal generation driven by the Auger 7 thermal generation mechanism (Piotrowski et al. 2010). A new strategy to achieve HOT detectors includes barrier structures launched by White and followed by Maimon and Wicks (White 1983; Maimon and Wicks 2006). Potential capability of the simple unipolar BIRD detector is that the generation-recombination (GR) current being dominated by the generation of electrons and holes by Shockley–Read–Hall (SRH) traps in the depletion region may be significantly suppressed by widegap (in relation to absorber and cap layer) barrier implementation to the detector's structure. Assuming that simple BIRD nB_nn detector is nearly lacking of depletion region

in active layer, the GR contribution to the net dark current from the absorber layer is limited. In low-temperature region (below crossover temperature), the nB_nn detector should exhibit a higher signal-to-noise ratio in comparison with a conventional p-n diode operating at the same temperature and should operate at a higher temperature with the same J_{DARK}.

Unipolar BIRD architecture was firstly implemented in $A^{III}B^{V}$ bulk materials (InAs, InAsSb), after in T2SLs e.g. InAs/GaSb and finally introduced into HgCdTe by Itsuno et al. in both mid- and long wave ranges (Klipstein 2008; Rodriguez et al. 2007; Itsuno et al. 2011). Growth of BIRD structure exhibiting no valence band offset (VBO) ≈ 0 eV between barrier and absorber for HgCdTe (MWIR HgCdTe—VBO < 200 meV depending on both absorber/barrier composition and doping, $T = 200$ K) has turned out to be difficult in terms of technology, however the research on this structures has been developing owing to problems with p-type doping in molecular beam epitaxy (MBE) technology. VBO in HgCdTe-based unipolar BIRD creates several issues limiting their performance. Depending on the wavelength of operation, a relatively high bias, typically greater than the bandgap energy (turn on voltage) is required to be applied to the device in order to collect the photogenerated carriers. This leads to strong band-to-band (BTB) and trap-assisted (TAT) tunneling due to the high electric field at the barrier absorber heterojunction. Proper interface doping at the cap-barrier and barrier absorber heterojunctions should lower VBO (Schubert et al. 1991). Parameters of the MCT devices are still better than devices employing other materials to include $A^{III}B^{V}$ based T2SLs InAs/GaSb. In spite of many advantages, HgCdTe is technologically extremely difficult to grow. Hg bonding reduces strength of a material, resulting in weak mechanical properties and creating difficulties in a material *processing*. Moreover, the high Hg vapor pressure makes the composition control over a large area difficult (Rogalski 2005).

Itsuno et al. (2012) presented nB_nn device being a prospect for circumventing of the p-type doping requirements in MBE technology related to an inconvenient ex situ As activation. Since HgCdTe p-type material is much more favorable, metalorganic chemical vapour deposition (MOCVD) growth allowing both in situ donor and acceptor doping seems to be more attractive in terms of growth of pB_pp HgCdTe barrier structures. Barrier structures with p-type doped constituent layers grown by MOCVD were presented by Kopytko et al. (2014). The paper presents comparison of the BIRD nB_nn and pB_pp HgCdTe detectors in terms of dark current and detectivity versus voltage, absorber doping, barrier Cd composition and doping.

2 Simulation procedure

Both nB_nn and pB_pp MWIR HgCdTe detectors were simulated with APSYS platform by Crosslight Inc. (APSYS 2014). The structural and simulation parameters were presented in Table 1 while modelled unipolar BIRD structure is shown in Fig. 2a. Interface barrier layers were assumed to be x-graded regions and represent the real structure which profile is shaped by interdiffusion processes during HgCdTe MOCVD growth.

Theoretical modeling of the MWIR HgCdTe barrier detectors has been performed by numerical solving of the Poisson's equation and the carrier current continuity equations by the Newton-Richardson method of nonlinear iterations (APSYS 2014). The applied model incorporates electrical properties to include the influence of radiative (RAD), Auger (AUG), SRH GR at any location within the device and BTB as well as TAT mechanisms at the barrier-absorber heterojunction. For the TAT simulation the Hurkx et al. (1992) model was implemented. We incorporated AUG recombination mechanisms using theory by Casselman and Petersen (1980). APSYS numerical platform requires the HgCdTe's composition,

Table 1 Parameters taken in modeling of MWIR nB$_n$n and pB$_p$p HgCdTe detectors

	Cap	Barrier	Absorber	n$^+$ contact
N_D/N_A [cm^{-3}]	$10^{14} \rightarrow 5 \times 10^{16}$	7×10^{14}, 10^{16}	$10^{14} \rightarrow 10^{17}$	2×10^{17} cm^{-3}
x_{Cd}	0.33	0.33 → (0.35 → 0.7) → 0.2863	0.2863 ($\lambda_c = 5\,\mu$m at $T = 200$ K)	0.2863
d[µm]	0.3	0.05 → 0.1 → 0.05	5	0.5
A[µm^2]		100 × 100		
Gauss tail, dx		0.02		
T_B, field of view, FOV		300 K, 20°		
$F_1 F_2$		0.15		
E_{Trap}		$E_g/2$		
N_{Trap}[cm^{-3}]		10^{14}		
SRH, τ_n, τ_p[µs]		10, 1		
Φ[W/m^2]		5		

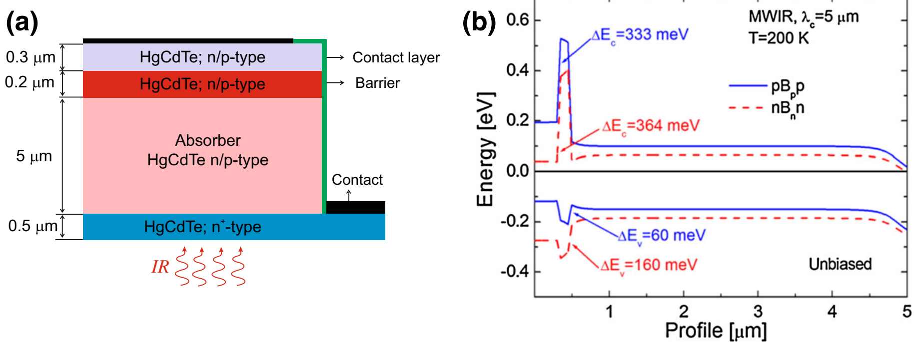

Fig. 2 Simulated nB$_n$n and pB$_p$p barrier structures (**a**); band diagrams for unbiased conditions for nB$_n$n and pB$_p$p BIRD detectors (**b**)

temperature and doping dependence of the electron affinity, bandgap, intrinsic concentration, mobility and effective masses. Bandgap was obtained from the paper by Hansen et al. (1982). The low-field electron mobility was taken after Scott's study, where the hole mobility was basically taken as 0.01 of the electron mobility (Scott 1972). The intrinsic concentration, composition and temperature dependence was calculated based on the Hansen and Schmidt (1983) model. Although HgCdTe exhibits a non-parabolic conduction band and high carrier degeneracy, computations were performed using the Fermi–Dirac statistics for a non-degenerate semiconductor model with parabolic energy bands (Quan et al. 2007; Wang et al. 2010, 2011). This simplification is valid for a wide range of doping concentrations (Wenus et al. 2001). Absorption was assumed in active region. Ohmic contacts were modeled as Dirichlet boundary conditions—electron and hole quasi-Fermi levels are equal and assumed to be at the voltage of biased electrode, i.e., $E_{fn} = E_{fp} = V$.

The noise current was simulated using the following expression that includes both the thermal Johnson-Nyquist noise and electrical shot noise contributions:

$$i_n(V) = \sqrt{(4k_BT/RA + 2qJ_{DARK})A}, \quad (1)$$

where A is the area of the detector, RA is the dynamic resistance area product, J_{DARK} is the dark current density, and k_B is the Boltzmann constant. Detectivity (D^*) limited by thermal Johnson-Nyquist noise and electrical shot noise could be expressed by relation (where, R_i current responsivity):

$$D^* = \frac{R_i}{i_n(V)}\sqrt{A}. \quad (2)$$

Both nB_nn and pB_pp detectors require that the valence bands of the three constituent layers line up closely to allow minority carrier transport between the absorber and contact layers. n^+ extra layer was added to assure proper contact properties to the p-type active layer in pB_pp barrier structure. Band diagram of the simulated structures is shown in Fig. 2b. The band energy discontinuity of both barrier layer and absorber layer seems to be the most decisive parameter influencing performance of barrier structure. Similarly to nB_nn, for pB_pp barrier in conduction band (ΔE_c) is higher compared to barrier in valence band ($\Delta E_c > \Delta E_v$) (see Fig. 2b). At equilibrium both ΔE_v (160 meV) and ΔE_c (364 meV) for nB_nn are higher in comparison to ΔE_v (60 meV) and ΔE_c (333 meV) for pB_pp, at $T = 200$ K. Dark and photocurrent are effectively blocked for ΔE_v; $\Delta E_c > 3k_BT \approx 50$ meV ($T = 200$ K).

J_{DARK} versus voltage is shown in Fig. 3a. pB_pp structure reaches lower dark current for > 175 mV. Cap layer's doping to the level of 5×10^{15} cm^{-3} and ΔE_c dependence on voltage is responsible for the J_{DARK} increase with bias, while for pB_pp J_{DARK} saturates. pB_pp structure allows operation for unbiased conditions being directly related to ΔE_v and ΔE_c dependence on voltage ($\Delta E_v < 3k_BT$).

Since both HgCdTe n/p-type barrier height in conduction band was estimated to be within the range of ~400 meV, the SRH GR contribution is evident in HOT conditions. Crossover temperature (T_C-temperature where diffusion component is balanced by GR component) for nB_nn was estimated at $T_C \approx 152$ K, while for pB_pp $T_C \approx 164$ K. (Fig. 3b. Barrier x_{Cd} composition influence on J_{DARK} and J_{PHOTO} is presented in Fig. 3c. Barrier x_{Cd} has no influence on J_{PHOTO} for pB_pp which indicates that ΔE_v has no influence on the transport of the photogenerated carriers, while for nB_nn this behavior is observed for $x_{Cd} > 0.5$. pB_pp J_{DARK} saturates reaching $\sim 3 \times 10^{-4}$ A/cm^2 for $x_{Cd} > 0.49$, while for nB_nn this effect is observed for $x_{Cd} > 0.66$.

nB_nn J_{DARK} and J_{PHOTO} versus absorber doping for two selected barrier doping $N_D = 7 \times 10^{14}$ and 10^{16} cm^{-3} are presented in Fig. 4a. For B-$N_D = 10^{16}$ cm^{-3}, J_{DARK} keeps constant ~ 10 A/cm^2 for absorber $N_D = 0.01 \rightarrow 1$ cm^{-3}, while above slight increase of the dark current is observed. For B-$N_D = 7 \times 10^{14}$ cm^{-3} J_{DARK} increases three orders of magnitude ($2 \times 10^{-3} \rightarrow 2$ A/cm^2), J_{PHOTO} stays constant to $N_D = 10^{16}$ cm^{-3}. Opposite trend is observed for J_{PHOTO} ($2 \times 10^{-1} \rightarrow 8 \times 10^{-5}$ A/cm^2) in analyzed active layer doping range. Figure 4b presents pB_pp J_{DARK} and J_{PHOTO} dependence on absorber doping for B-$N_A = 7 \times 10^{14}$ cm^{-3}. J_{PHOTO} stays constant for analyzed absorber doping range, while J_{DARK} increases sharply for $N_D > 10^{16}$ cm^{-3}.

Detectivity calculated according to relation (1) versus temperature is presented in Fig. 5a. nB_nn reaches background limited photodetector (BLIP) conditions at ~175 K, while for pB_pp at ~200 K. D^* for BLIP condition was calculated for background temperature, $T_B = 300$ K and field of view, $FOV = 20°$. Detectivity dependence on barrier composition is presented

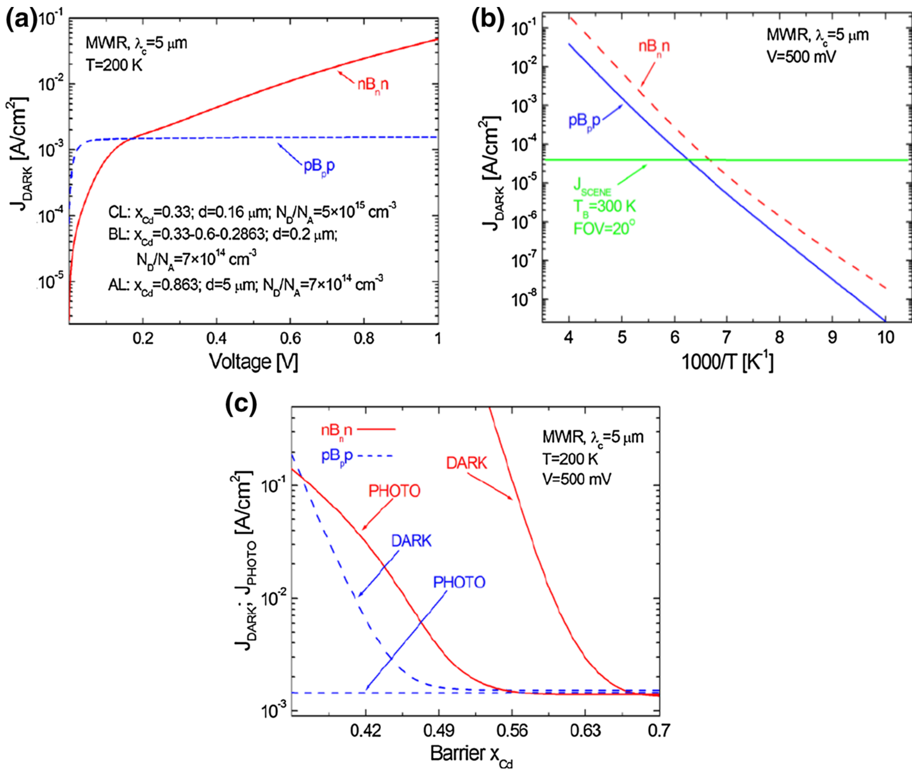

Fig. 3 J_{DARK} versus voltage (**a**); versus reciprocal temperature (**b**); J_{DARK} and J_{PHOTO} versus barrier Cd composition (**c**) for nB$_n$n and pB$_p$p barrier structures

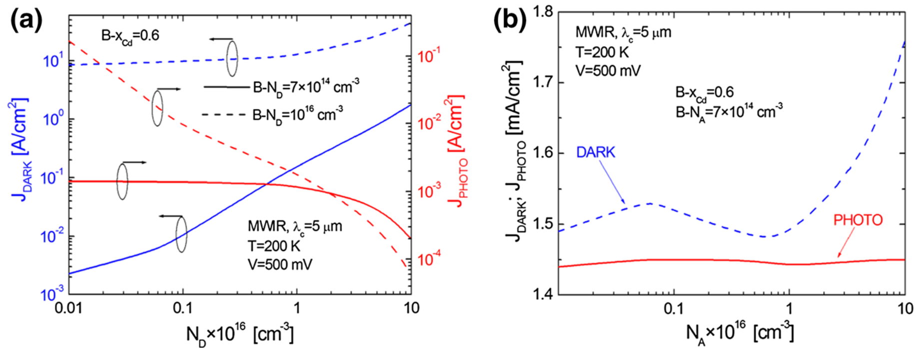

Fig. 4 J_{DARK} versus voltage $N_{D/A}$ for nB$_n$n (**a**) and pB$_p$p (**b**) barrier structures

in Fig. 5b. Barrier x_{Cd} should be higher than 0.49 for pB$_p$p structure, where D^* saturates, while for nB$_n$n, D^* increases with x_{Cd} (for $x_{Cd} > 0.49$). D^* versus active layer doping for two selected barrier's doping, B-$N_{D/A} = 7 \times 10^{14}$ and $10^{16}\,\text{cm}^{-3}$ (barrier $x_{Cd} = 0.6$) are presented in Fig. 5c. For absorber's N_D within $10^{14} \rightarrow 10^{17}\,\text{cm}^{-3}$, D^* decreases almost four orders of magnitude. Barrier doping also influences D^* (the higher barrier doping the lower D^* may be reached for $N_D > 2 \times 10^{14}\,\text{cm}^{-3}$, while below oppo-

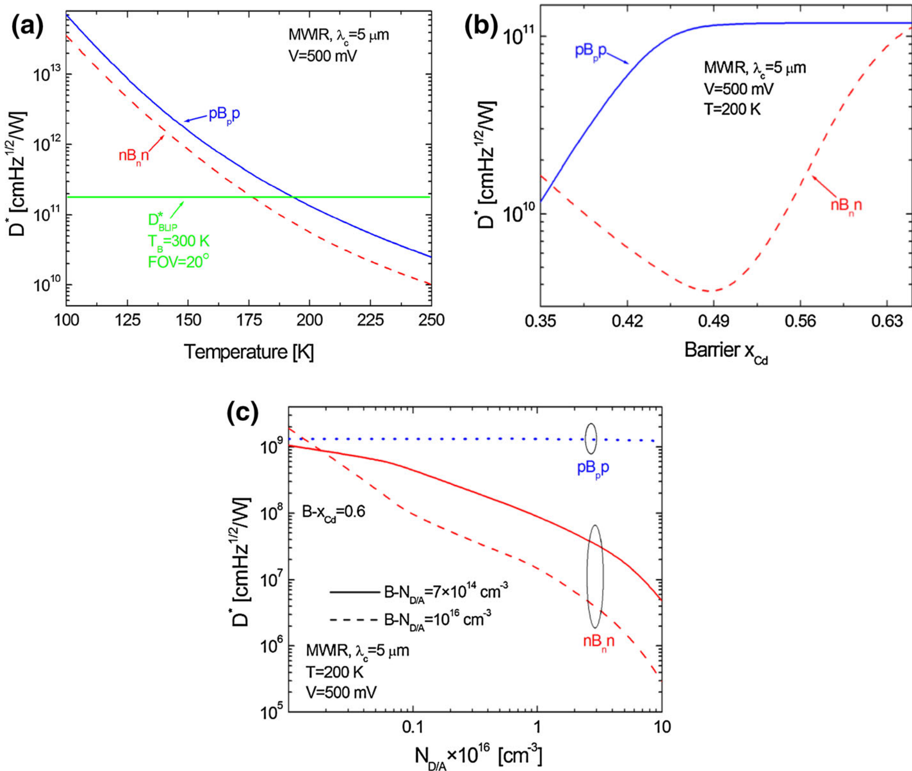

Fig. 5 D^* versus temperature (a); barrier composition (b) and absorber's doping $N_{D/A}$ (c) for nB_nn and pB_pp barrier detectors

site trend is observed). D^* for nB_nn ($\sim 10^8$ cm Hz$^{1/2}$/W) and pB_pp ($\sim 10^9$ cm Hz$^{1/2}$/W) BIRD structures could be increased by nearly 10 times by growth of the structures on GaAs substrates.

3 Conclusion

The barrier structure has been introduced to simplify the detector fabrication process and increase detector's operating temperature. Depending on the growth method, particular HgCdTe barrier architectures are favorable nB_nn - MBE, both nB_nn and pB_pp - MOCVD. pB_pp architecture allows to reach higher performance at MWIR spectrum for wide range of absorber doping $N_{D/A} = 2 \times 10^{14} \rightarrow 10^{17}$ cm^{-3} and barrier x_{Cd} composition. Simulations indicate that pB_pp structure is not that sensitive to the barrier and absorber doping changes in comparison to nB_nn detector. Further strategy in development of HgCdTe BIRD detectors should focus on decreasing or even removing the VBO at the barrier-absorber heterojunction, which will result in lower operating bias, lower dark current, and ability to operate at higher temperatures. Theoretically estimated D^* for both nB_nn and pB_pp BIRD detectors could possibly reach $\sim 10^9$ and $\sim 10^{10}$ cmHz$^{1/2}$/W by growth on GaAs substrates.

Acknowledgments We acknowledge support by National Centre of Research and Development—the Grant No. PBS 1/B5/2/2012.

Open Access This article is distributed under the terms of the Creative Commons Attribution License which permits any use, distribution, and reproduction in any medium, provided the original author(s) and the source are credited.

References

APSYS Macro/User's Manual ver. 2014. Crosslight Software, Inc. (2014)

Ashley, T., Elliott, C.T.: Non-equilibrium mode of operation for infrared detection. Electron. Lett. **21**, 451–452 (1985)

Casselman, T.N., Petersen, P.E.: A comparison of the dominant Auger transitions in p-type (HgCd)Te. Solid State Commun. **33**, 615–619 (1980)

Hansen, G.L., Schmidt, J.L., Casselman, T.N.: Energy gap versus alloy composition and temperature in $Hg_{1-x}Cd_xTe$. J. Appl. Phys. **53**, 7099–7101 (1982)

Hansen, G.L., Schmidt, J.L.: Calculation of intrinsic carrier concentration in $Hg_{1-x}Cd_xTe$. J. Appl. Phys. **54**, 1639–1640 (1983)

Hurkx, G.A., Klaassen, D.B.M., Knuvers, M.P.G.: A new recombination model for device simulation including tunneling. IEEE Trans. Electron. Devices **39**(2), 331–338 (1992)

Itsuno, A.M., Phillips, J.D., Velicu, S.: Design and modeling of HgCdTe nBn detectors. J. Electron. Mater. **40**(8), 1624–1629 (2011)

Itsuno, A.M., Phillips, J.D., Velicu, S.: Mid-wave infrared HgCdTe nBn photodetector. Appl. Phys. Lett. **100**, 161102 (2012)

Klipstein, P.: XBn' barrier photodetectors for high sensitivity and high operating temperature infrared sensors. Proc. SPIE **6940**, 69402U-1–69402U-11 (2008)

Kopytko, M., Jóźwikowski, K., Rogalski, A.: Fundamental limits of MWIR HgCdTe barrier detectors operating under non-equilibrium mode. Solid State Electron. **100**, 20–26 (2014)

Maimon, S., Wicks, G.: nBn detector, an infrared detector with reduced dark current and higher operating temperature. Appl. Phys. Lett. **89**, 151109-1–151109-3 (2006)

Norton, P.: HgCdTe infrared detectors. Opto-Electron. Rev. **10**, 159–174 (2002)

Piotrowski, J., Rogalski, A.: Uncooled long wavelength infrared photon detectors. Infrared Phys. Technol. **46**, 115–131 (2004)

Piotrowski, J., Rogalski, A.: High Operation Temperature Photodetectors. SPIE, Bellingham (2007)

Piotrowski, A., Madejczyk, P., Gawron, W., Klos, K., Pawluczyk, J., Rutkowski, J., Piotrowski, J., Rogalski, A.: Progress in MOCVD growth of HgCdTe heterostructures for uncooled infrared photodetectors. Infrared Phys. Technol. **49**, 173–182 (2007)

Piotrowski, J., Gawron, W., Orman, Z., Pawluczyk, J., Klos, K., Stępień, D., Piotrowski, A.: Dark currents, responsivity and response time in graded gap HgCdTe structures. Proc. SPIE **7660**, 766031 (2010)

Quan, Z.J., Chen, X.S., Hu, W.D., Ye, Z.H., Hu, X.N., Li, Z.F., Lu, W.: Modeling of dark characteristics for long-wavelength HgCdTe photodiode. Opt. Quantum Electron. **38**, 1107–1113 (2007)

Rodriguez, J.B., Plis, E., Bishop, G., Sharma, Y.D., Kim, H., Dawson, L.R., Krishna, S.: nBn structure based on InAs/GaSb type-II strained layer superlattices. Appl. Phys. Lett. **91**, 043514 (2007)

Rogalski, A.: HgCdTe infrared detector material: history, status and outlook. Rep. Prog. Phys. **68**, 2267–2336 (2005)

Rogalski, A.: Infrared Detectors, 2nd edn. CRC Press, Boca Raton (2011)

Schubert, E.F., Tu, L.W., Zydzik, G.J., Kopf, R.F., Benvenuti, A., Pinto, M.R.: Elimination of heterojunction band discontinuities by modulation doping. Appl. Phys. Lett. **60**, 466–468 (1991)

Scott, W.: Electron mobility in $Hg_{1-x}Cd_xTe$. J. Appl. Phys. **43**, 1055–1062 (1972)

Wang, J., Chen, X.S., Wang, Z.Q., Hu, W.D., Lu, W., Xu, F.Q.: The mechanism of the photoresponse blueshifts for the n-type conversion region of n^+-on-p $Hg_{0.722}Cd_{0.278}Te$ infrared photodiode. J. Appl. Phys. **107**, 044513 (2010)

Wang, J., Chen, X., Hu, W., Wang, L., Chen, Y., Lu, W., Xu, F.: Different approximation for carrier statistic in non-parabolic MWIR HgCdTe photovoltaic devices. Proc. SPIE **8012**, 80123B (2011)

Wenus, J., Rutkowski, J., Rogalski, A.: Two-dimensional analysis of double-layer heterojunction HgCdTe photodiodes. IEEE Trans. Electron. Devices **48**, (7), 1326–1332 (2001)

White A.: Infrared detectors, US. Patent 4,679,063 (1983)